ASTM INTERNATIONAL

Materials Performance and Characterization

S. Devaraj,[1] R. Kumar,[2] and S. Sankaran[2]

DOI: 10.1520/MPC20150011

Electric Erosion Induced Microstructure and Mechanical Properties in Spark Plasma Sintered Al-4.5 wt. % Cu Alloy

VOL. 5 / NO. 1 / 2016

Materials Performance and Characterization

doi:10.1520/MPC20150011 / Vol. 5 / No. 1 / 2016 / available online at www.astm.org

S. Devaraj,[1] R. Kumar,[2] and S. Sankaran[2]

Electric Erosion Induced Microstructure and Mechanical Properties in Spark Plasma Sintered Al-4.5 wt. % Cu Alloy

Reference

Devaraj, S., Kumar, R., and Sankaran, S., "Electric Erosion Induced Microstructure and Mechanical Properties in Spark Plasma Sintered Al-4.5 wt. % Cu Alloy," *Materials Performance and Characterization*, Vol. 5, No. 1, 2016, pp. 54–65, doi:10.1520/MPC20150011. ISSN 2165-3992

ABSTRACT

The Al-4.5 wt.% Cu powder was compacted by spark plasma sintering at three compaction pressures namely 30, 40, and 50 MPa maintaining temperature constant at 500°C. Porosity seems to be closed in all the 3 cases. Relative density of S-50 is decreased due to increase in electrical erosion holes. Transmission electron microscopy studies reveal the presence of dislocations in all the compacts and shear bands observed only in the compact sintered at 50 MPa. A power law creep mechanism involving dislocations is found to be observed in all the compacts sintered at all pressures, which is evident from the TEM micrographs as well. The dissolution of Al_2Cu precipitates in the aluminum matrix, and the increase in electric erosion holes were noticed with increase in pressure from 30 to 50 MPa. The decrease in the volume fraction of Al_2Cu phase and the increase in the formation of electric erosion holes resulted in reduced hardness and compression strengths of the compacts.

Keywords

spark plasma sintering, mechanism, microstructure, electric erosion hole, hardness, compression strength

Manuscript received March 16, 2015; accepted for publication December 14, 2015; published online March 10, 2016.

[1] Department of Mechanical Engineering, SJC Institute of Technology, Chickballapur, 562101 India (Corresponding author), e-mail: devarajsiim@gmail.com

[2] Department of Metallurgical and Materials Engineering, Indian Institute of Technology Madras, Chennai 600036, India.

Introduction

Al-4.5 wt. % Cu alloy is an age hardenable alloy extensively used in aeronautical and automobile industries [1,2]. Improved versions of AA2024 alloy exhibits higher toughness, high resistance to cyclic loading, and high strength. These alloys are particularly useful in aerospace structural applications such as wing tension members, shear webs, and ribs. The alloys were strengthened by ageing through the different precipitation sequence [3]. Traditionally, different processing routes such as ingot metallurgy and powder metallurgy have been employed to enhance the mechanical properties of this alloy by affecting the grain size and the distribution of Al_2Cu phase within the aluminum matrix [4,5]. The alloys produced through a casting route are easy, straight forward, and cooling rate during the solidification is relatively slow [6]. On the contrary, alloys produced by rapid solidification techniques, such as spray deposition and powder metallurgy, exhibit refined microstructures resulting in enhancement of the mechanical properties [7]. Powder metallurgy route with conventional sintering process is tedious and involves numerous processing steps [8]. Spark plasma sintering (SPS) is a relatively new and promising powder consolidation technique that offers relatively high heating rates and less sintering time [9,10].

Schubert et al. [11] examined Al-Si alloys produced by SPS method sintered at temperature of 450°C at a pressure of 170 MPa for a holding time of 10 min. The SPS results were compared with hot extruded material. The results exemplified superior tensile properties of the hot extruded material in contrast to the SPS processed compact. This was attributed to some residual porosity present at the peripheral region. Wang et al. [12] reported on the influence of direct electric current on plasma activated sintering copper powder compact. The high electric current involved in the process enhance the densification rate, whereas constant electric current and high mechanical pressure employed during the sintering process exhibits lower densification rate [12]. Tokita [13] reported that the microstructural changes in a sintered (SPS) bronze alloy. The results showed that the neck formation was due to spark plasma generated during the SPS process.

Zhaohui et al. [14] proposed the four stages mechanism for sintering of the copper powder in the following sequence: (1) activation of the powder due to joule heating; (2) neck formation; (3) neck growth; and (4) plastic deformation of the particle. The first and the second stages indicate the local heating, activation, and neck formation of the powder. In the third and fourth stages, powder was subjected to neck growth and plastic deformation by mass transporting of the materials. In order to obtain high quality densified bulk compact, the plastic deformation of the particle plays a major role for mass transport. High pressure was applied during the sintering process as well as holding period of the SPS process [14]. Munir et al. [15] reported the significant role of applying mechanical pressure during the SPS process. The applied pressure has two roles: one is a mechanical role and the other is an intrinsic role. The mechanical role helps in rearrangement of particles and the intrinsic role depends on size of the particle. The contribution of the pressure is high when the particle size is large and becomes less significant as the size is decreased. It is observed that the applied pressure has no role to play on grain size [15]. Olevsky et al. [16] developed a theoretical model to show the contribution of mass transfer by grain boundary diffusion and power law creep mechanism. It was shown that for

a grain size of 40 μm, the power-law mechanism is operative, whereas for the grain size of 1 μm and 100 nm particles, electromigration and sintering stress were found to play an important role for the material transport.

From the available literature, it is clear that attempts to sinter metallic powder particles by spark plasma sintering have been made to study the influence of sintering pressure on microstructural and mechanical behavior, while a comprehensive analysis of the influence of sintering pressure on the microstructure and mechanical properties of Al-4.5 wt. % Cu is lacking. Therefore, in the present work, the Al-4.5 wt. % Cu alloy powder was compacted at various pressures. The microstructural variation as a function of the pressure applied during sintering and its effect on mechanical properties are discussed.

Experimental

Al-4.5 wt. % Cu alloy powder was obtained during spray atomization in a nitrogen atmosphere. The coarse powder particles were separated by sieve analysis, and subsequently the size distribution of the powder particles were measured using Microtrac S3500 laser particle analyser, USA. The powder particles ranging from 25 to 350 μm were chosen for spark plasma sintering (SPS). The powder particles were placed inside the graphite die of 30 mm inner diameter. On either side of the powder, the graphite foils were kept inside the die before placing the graphite punches. The powder loaded graphite die and punches were placed between the spacers. In order to measure the temperature of the die, the R type thermocouple was inserted into a hole provided on the outer surface of the die. A high pulsed current (1660 A) and low voltage (2.76 V) was applied using a spark plasma sintering machine (Dr. Sinter 1050, Japan). During the sintering process, the sintering data were recorded from the data acquisition system. Three SPS compacts were sintered at varying pressures of 30, 40, and 50 MPa at a constant sintering temperature of 500°C. The other parameters such as heating rate (50°C/min), holding time (5 min) was kept constant. The size of the sintered compacts was 300 mm in diameter and ~10 mm in thickness. The density of the samples was measured using water displacement method. The aforementioned compacts, hereafter, are referred as S-30, S-40, and S-50 in the article. For microstructural analysis, small pieces were cut from the sintered compacts, polished to a mirror finish according to the standard metallographic procedure and were etched with Keller's reagent. For TEM analysis, the SPS samples were thinned down to less than 100 μm thickness by polishing on smooth emery sheet. The thinned sample of 3 mm diameter was cut from the foil and was polished by twin jet polisher using nitric acid and methanol in 1:3 ratios. The microstructural analysis was carried out using optical microscopy (Leitz laborex 12 ME, Germany), scanning electron microscopy (FEI Quanta 200) and the transmission electron microscopy (Philips CM 12, the Netherlands). The phases of the SPS compact were analyzed using AXS X-ray diffractometer (D8 Discover, Bruker, USA). The hardness of the sintered compacts was measured using bulk Vickers hardness tester (WOLPERT 402 MVD, USA). The rectangular samples (4 by 4 by 8 mm) for compression tests were prepared according to ASTM E9-09 [17] standards. The compression strength of the SPS compacts was investigated by INSTRON 3367 compression machine at the strain rate of 0.18×10^{-3} s^{-1}.

FIG. 1
Microstructures of powder (a) variety of the atomized powder and (b) cellular and dendritic morphology of the powder particle.

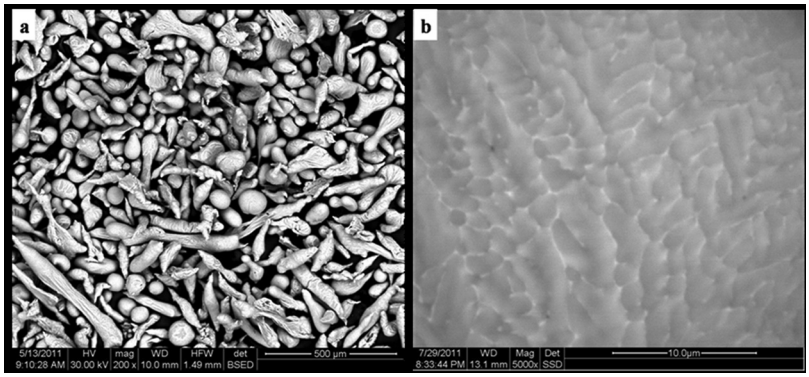

Results and Discussion

MICROSTRUCTURAL CHARACTERIZATION

The morphological details of powder particles (spherical, elongated, and irregular type) and the distribution of Al_2Cu phases located along the cell boundaries are shown in **Fig. 1(a)** and **1(b)**, respectively, and also detailed in an earlier publication [18].

The cooling rates of smaller and spherical powder particles were high due to increased surface area to volume ratio and hence exhibited cellular microstructure. Elongated and irregular shaped powder particles exhibit both cellular and dendritic microstructures due to possible reduction in cooling rates. The powder particle size distribution of Al-4.5 wt. % Cu alloy powder is shown in **Fig. 2**.

A wide distribution in size varying from size of 25 to 350 μm with maximum size in the range of 75–100 μm is observed. The size of the powder particles plays a major role in the distribution of the secondary phase and the porosity of the sintered compacts. The relative densities of S-30, S-40, and S-50 are 99, 98, and 96 %, respectively. The relative densities of the compacts decreased with increase in sintering pressure from 30 to 50 MPa due to increase in electric erosion holes. A relative

FIG. 2
Powders size distribution.

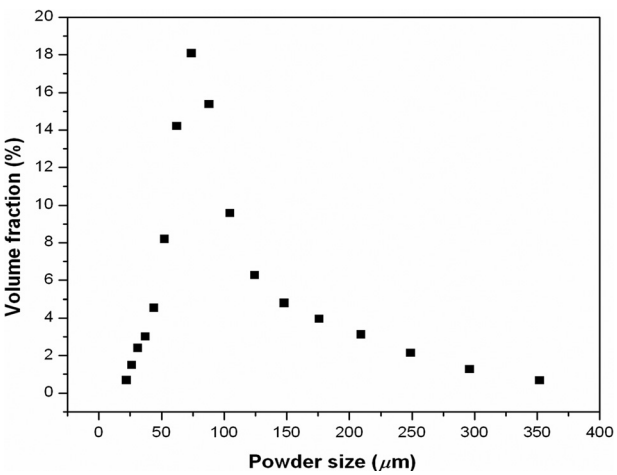

FIG. 3
X-ray diffractograms exemplifying aluminum and Al_2Cu phase.

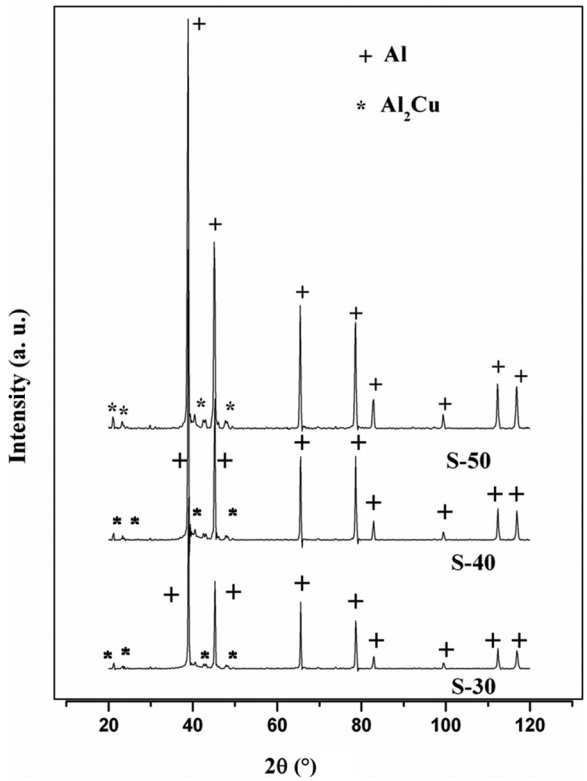

density of 99 % is achieved for S-30, whereas the relative density of S-50 decreased to 96 %. The decrease in relative density of S-50 could be attributed to the increase in formation of erosion holes induced during sintering at higher pressure and temperature. In all the three compacts, porosity of less than 1 % was observed. The phases present in the SPS compacts were analyzed and the X-ray diffractogram shown in **Fig. 3** confirms the presence of aluminum and Al_2Cu phase in all three the compacts.

FIG. 4
Micrographs showing the grain boundaries and distribution of Al_2Cu phase inside the grains and along the grain boundaries, (a) S-30 and (b) corresponding high magnified image.

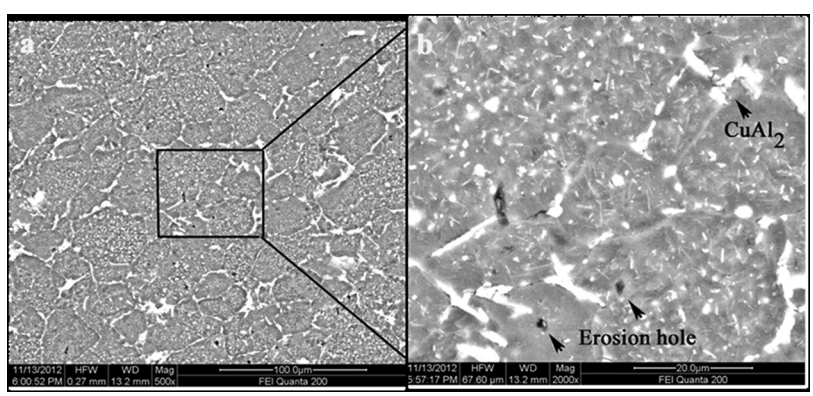

FIG. 5
Micrographs showing the grain boundaries and distribution of Al_2Cu phase inside the grains and along the grain boundaries, (a) S-40 and (b) corresponding high magnified image.

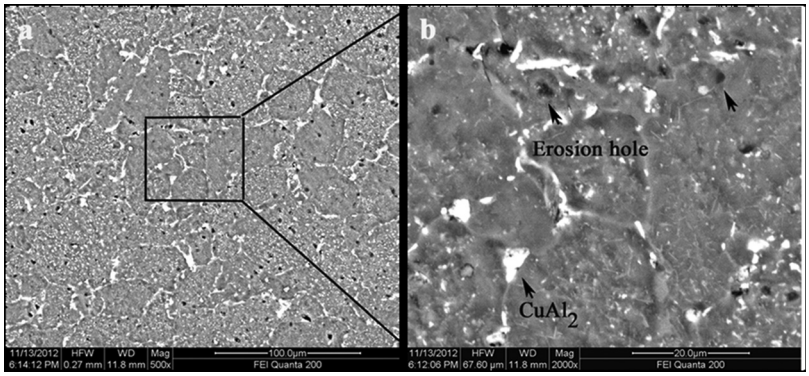

Figs. 4, **5** and **6** indicate the typical micrographs of S-30, S-40, and S-50 microstructures exemplifying the consolidation of the powder particles after sintering and the distribution of Al_2Cu phase.

The morphology of the powder particles seemed to change due to the combination of the high temperature and pressure applied during the SPS process. The material is subjected to high plastic deformation as a result of which brittle Al_2Cu phase disintegrate into a number of individual particles and distributed uniformly within the grains and along the grain boundaries. The volume fraction of Al_2Cu phase reduced (**Fig. 6**) with increase in pressure from 30 to 50 MPa due to a possible dissolution of the phase.

ELECTRIC EROSION HOLES

The SEM micrographs (**Figs. 4**–**6**) show the electrical erosion holes formed during the sintering process due to high intensity of pulsed current and are increased with increase in pressure. The schematic shown in **Fig. 7** typifies the formation of electric erosion holes during the SPS process at high temperature and pressure.

At the initial stages of spark plasma sintering, the arcs are produced between the powders (**Fig. 7(a)**) due to the pulsed current passed through the powder.

FIG. 6
Micrographs showing the dissolution of Al_2Cu phase inside the grains and along the grain boundaries, (a) S-50 and (b) corresponding high magnified image.

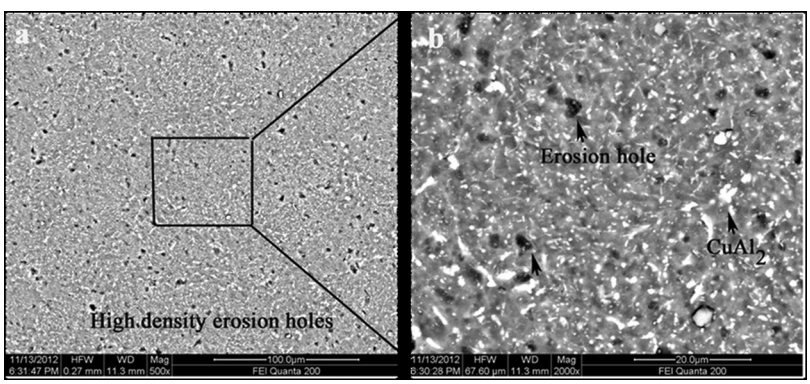

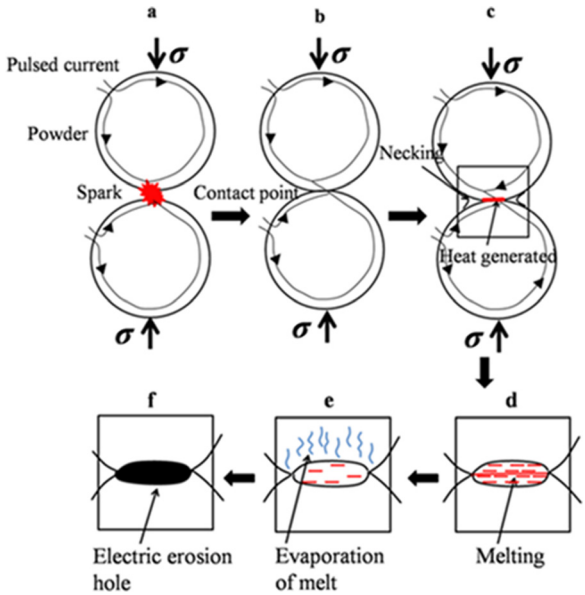

FIG. 7
Schematic diagram showing formation of electric erosion holes (a) spark between the powder and (b) contacts points established between the powders, (c) heat generated at the contact points, (d) melting zone at the contact, (e) evaporation of the melt, and (f) formation of electric erosion hole.

The ionized gases are liberated around the powder particles and helps in activating the powder by eliminating the oxide film on the outer surface of the powder. The gap between the powder particles is reduced and contacts between them (**Fig. 7(b)**) are established as the pressure is increased. When the gap between the powders is reduced, the spark jumps across the powder and the discharge pulsed current is converted into heat. A large amount of heat is generated (**Fig. 7(c)**) at the contact points due to high pulsed current passing through the powder. This means that the high pulsed current is converted to a large amount of heat at the contact points. This result in melting the powder at the contact points and the melt starts evaporating (**Fig. 7(d)**). On further increasing the pressure, more melt gets evaporated (**Fig. 7(e)**) at the contact points than the surface of the powder due to large amount of heat at the contact points. This results in the formation of craters at the contact points of the powder. The craters formed due to high pulsed current results in electric erosion holes (**Fig. 7(f)**). Such electric erosion holes increased with increase in the sintering pressure from 30 to 50 MPa. The evaporation of the liquid at the outer surface of the powder increased by increasing the pressure of the compact thereby increasing the electric erosion holes, which is clearly evident from the microstructure of S-50 (**Fig. 6**).

TEM MICROSTRUCTURES

The TEM results of S-30, S-40, and S-50 are shown in **Figs. 8(a)** and **8(b)**, **8(c)**, **8(d)**, and **8(e)** and **8(f)**, respectively.

The TEM results correspond well with X-ray diffraction result exemplifying the presence of Al_2Cu precipitates in the aluminum matrix. The spherical and plate shaped Al_2Cu particles are clearly observed in TEM micrographs (**Figs. 8(a)**,

FIG. 8 Bright field micrographs of S-30 (Figs. a and b), S-40 (Figs. b and c) and S-50 (Figs. d and e) (a) presence of Al_2Cu precipitates and dislocation cells, (b) Interaction of dislocation with Al_2Cu precipitate along the grain boundary, (c) different grains and dislocation substructures, (d) grain boundary with dislocation, (e) small grains with dislocation substructures and Al_2Cu precipitates, and (f) presence of shear bands.

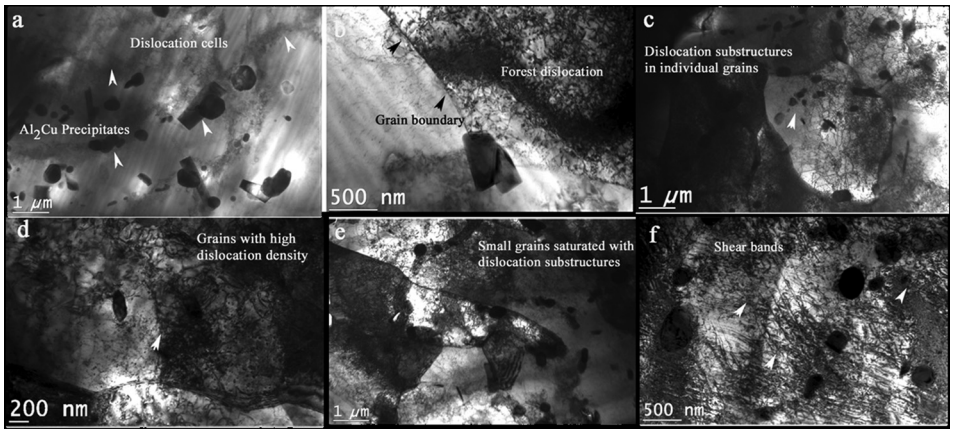

8(c), and 8(e)). The interaction of dislocations with the precipitates and the pile up of the dislocations at the grain boundaries are visible in **Figs. 8(b)** and **8(d)**, and it is evident that the dislocations are generated during the SPS process. It is evident from the TEM micrographs (**Fig. 8(b)**) that dislocations are responsible for mass transportation indicating the power-law creep mechanism to be operative during the sintering process reported in the present work. Prabir and Farghalli [19] investigated that the creep behavior of a Al-3.0 Cu alloy in the temperature range of 500°C–580°C, with stresses varying between 0.3 to 1.5 MPa, exhibits a stress exponent $n \sim 4.5$ [19]. Kloc et al. [20] examined that 2024 alloy over a temperature range of 250°C–330°C and stresses in the range of 25–50 MPa exhibited a stress exponent ~ 5 related to a dislocation based creep mechanism considered to be dominant [20]. Under high pressure of 50 MPa at 500°C, the material is subjected to severe plastic deformation. The shear bands produced due to severe plastic deformation during the SPS process at high temperature and pressure is confirmed by TEM images (**Fig. 8(f)**).

DENSIFICATION MECHANISMS

Zhaohui et al. [14] described sintering mechanism and the effect of pulsed current on Cu powder during the SPS process. The intensity of the spark generated between the Cu powder particles is weak at the initial stages of the pulsed current. However, the local temperature between the powder particles was higher than the tested temperature due to the spark generated between the gaps of the powder. Due to localized melting, the oxide layers on the powder have been removed and, consequently, the powder has been refined and activated. During the refining process, the electric erosion holes were formed due to high intensity of pulsed current. The outer surfaces of the powder were softened because of localized melting and the binding force between the Cu atoms was weakened results in increasing

FIG. 9 Densification mechanism plots during SPS process, (a) S-30, (b) S-40, and (c) S-50.

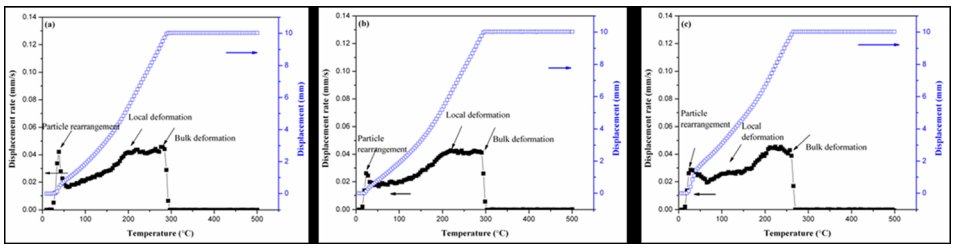

the diffusivity of the Cu atoms. Therefore, necks were formed and grew further while transporting the material. Once the necks were formed, the spark discharged between the powders stopped and high density pulsed current passing through the necks resulted in densification of the compact. The compact densified quickly because of rapid increase in temperature.

Devaraj et al. [18] explained the similar sintering curves of wide range of powder from 25 to 500 μm for different temperatures of 400, 450, and 500°C at constant pressure of 30 MPa. The curves described the mechanisms such as particle rearrangement, local deformation, and bulk deformation for a wide range of powder 25 to 500 μm. The study was also focused on displacement of narrow range and wide range of powder during sintering process at constant pressure. From the sintering curves, it was evident that displacements of wide range of powder occur in two stages, whereas for narrow range of powder, the displacement of powder occurs only in single stage. It was found that good quality and the highly sintered compact was obtained when the powder sintered at 500°C under a pressure of 30 MPa [18]. Similarly, attempts are made to draw the sintering curves of wide range of powder from 25 to 350 μm for different pressures of 30, 40, and 50 MPa at a constant temperature of 500°C. The densification curves drawn for different pressures are shown in **Fig. 9**.

In this curve, the powder particles are rearranged in a single stage. In S-30 and S-40 the deformation of material starts approximately at 300°C, whereas for S-50 the bulk deformation starts approximately at 260°C. In this case, there is sufficient time and temperature available for plastic deformation resulting in deformation bands (**Fig. 8(f)**).

MECHANICAL CHARACTERIZATION

The Vickers bulk hardness of S-30, S-40, and S-50 are 698 ± 15, 647 ± 15, and 605 ± 10 MPa, respectively. From the experimental results, it is confirmed that, there is an adverse effect of pressure on hardness at higher pressures. The pressure helps only in rearrangement of particles during the sintering process. The marginal amount of decrease in hardness from S-30 to S-50 could be attributed to dissolution of precipitates at higher pressures at the sintering temperature of 500°C. The compression true stress-true strain curves are shown in **Fig. 10**.

FIG. 10

Compression true stress-true strain curves of S-30, S-40 and S-50.

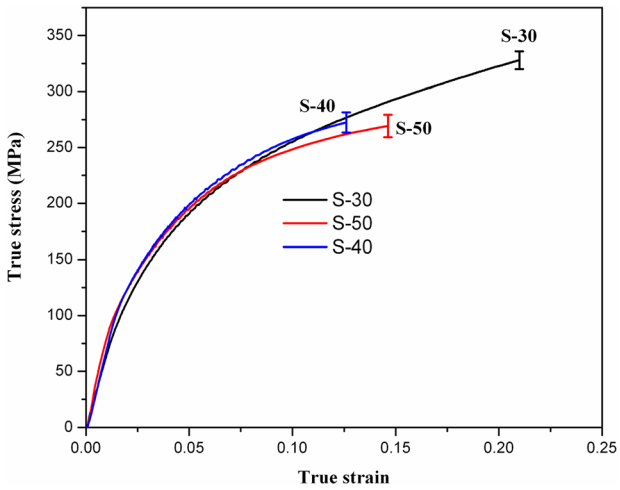

The compression strength of S-30, S-40, and S-50 are 327 ± 8, 274 ± 10, and 272 ± 9 MPa, respectively. The compression test results indicated that the S-30 exhibit relatively high compression strengths in contrast to S-40 and S-50. The Al_2Cu phase disintegrates into number of individual particles (**Fig. 4(a)**) and obviously the disintegrated particles exhibits higher strength. Furthermore, the presence of high dislocations density shown in **Fig. 8(b)** and the interaction of dislocations with the precipitates enhance the strength of the alloy. When the pressure is increased from 30 to 50 MPa, the disintegrated secondary phase dissolved into aluminum matrix. In contrast to **Fig. 4(a)**, the dissolution of Al_2Cu phase can be seen clearly from the **Figs. 5(a)** and **6(a)**. In addition, the formation of electric erosion holes also plays a major role in decreasing the hardness and the compression strength. As the pressure is increased, the electric erosion holes also increased resulting in the compromise of the mechanical properties. The increase in the formation of electric erosion holes of S-50 (**Fig. 6(b)**) has an adverse effect on ultimate compression strength as well.

Conclusions

This study focused on microstructural and mechanical characterization of the spark plasma sintered Al-4.5 wt. % Cu powder at varied pressures sintered at a constant temperature of 500°C. With increase in the pressure from 30 to 50 MPa, more of Al_2Cu precipitates seem to dissolve in the aluminum matrix. The decrease in the volume fraction of the secondary phase (Al_2Cu) and increase in electric erosion holes resulted in the degradation of the mechanical properties. The Vickers macrohardness and compression strengths of the sintered compacts processed at 30 MPa are 14 and 17 % higher than the compact sintered at 50 MPa. The relatively higher hardness and compression strength observed in S-30 is attributed to the high volume fraction of the Al_2Cu phase with minimal electric erosion holes in contrast to S-40 and S-50.

References

[1] Guinier, A., "Heterogeneities in Solid Solutions," *Solid State Phys.*, Vol. 9, 1959, pp. 293–398.

[2] Gläser, U. H., Dlubek, G., and Krause, R., "Vacancies and Precipitates in Al–1.9 at% Cu Studied by Positrons," *Phys. Status Solidi B.*, Vol. 163, No. 2, 1991, pp. 337–343.

[3] Wang, S. C. and Starink, M. J., "Precipitates and Intermetallic Phases in Precipitation Hardening Al–Cu–Mg–(Li) Based Alloys," *Int. Mater. Rev.*, Vol. 50, No. 4, 2005, pp. 193–215.

[4] Brody, H. D. and Flemings, M. C., "Solute Redistribution in Dendritic Solidification," *Trans. Met. Soc. AIME.*, Vol. 36, Nos. 3–4, 1966, pp. 615–623.

[5] Singer, A. R. E., "Principles of Spray Deposition," *Met. Mater.*, Vol. 4, No. #, 1970, pp. 246–255.

[6] Kattamis, T. Z., Coughlin, J. C., and Flemings, M. C., "Influence of Coarsening on Dendrite Arm Spacing of Aluminum-Copper Alloys," *Trans. Met. Soc. AIME*, Vol. 236, 1967, pp. 1504–1511.

[7] Ojha, S. N. and Singh, S. N., "On Spray Deposition of High-Speed Steel," *J. Mater. Sci. Lett.*, Vol. 10, No. 15, 1991, pp. 893–895.

[8] Lee, S. M., Jung, J. H., Fleury, E., Kim, W. T., and Kim, D. H., "Metal Matrix Composites Reinforced by Gas-Atomised Al-Cu-Fe Powders," *Mater. Sci. Eng. A.*, Vols. 294–296, 2000, pp. 99–103.

[9] Xie, G., Ohashi, O., Song, M., Mitsuishi, K., and Puruya, K., "Reduction Mechanism of Surface Oxide Films and Characterization of Formations on Pulse Electric-Current Sintered Al–Mg Alloy Powders," *Appl. Surf. Sci.*, Vol. 241, Nos. 1–2, 2005, pp. 102–106.

[10] Goldberger, W. M., Merkle, B., and Boss, D., "Making Dense Near Net Shaped Parts by Electro Consolidation," *Adv. Powder. Metall. Part. Mater.*, Vol. 6, No. #, 1994, pp. 91–102.

[11] Schubert, T., Schmidt, J., Weissgärber, T., and Kieback, B., "Microstructure and Mechanical Properties of an Al-Si Alloy Consolidated by Spark Plasma Sintering," *Proceedings of the 2010 World Congress-Spark Plasma Sintering*, Dresden, Germany, 28, D-01277.

[12] Wang, S. W., Chen, L. D., Kang, Y. S., Niino, M., and Hirai, T., "Effect of Plasma Activated Sintering (PAS) Parameters on Densification of Copper Powder," *Mater. Res. Bull.*, Vol. 35, No. 4, 2000, pp. 619–628.

[13] Tokita, M., "Trends in Advanced SPS Spark Plasma Sintering Systems and Technology," *J. Soc. Powder Technol. Jpn.*, Vol. 30, No. 11, 1993, pp. 790–804.

[14] Zhaohui, Z., Fuchi, W., Lin, W., Shukui, L., and Osamu, S., "Sintering Mechanism of Large-Scale Ultrafine-Grained Copper Prepared by SPS Method," *Mater. Lett.*, Vol. 62, No. 24, 2008, pp. 3987–3990.

[15] Munir, Z. A., Anselmi-Tamburini, U., and Ohyanagi, M., "The Effect of Electric Field and Pressure on the Synthesis and Consolidation of Materials: A Review of the Spark Plasma Sintering Method," *J. Mater. Sci.*, Vol. 41, No. 3, 2006, pp. 763–777.

[16] Olevsky, E. and Froyen, L., "Constitutive Modeling of Spark-Plasma Sintering of Conductive Materials," *Scr. Mater.*, Vol. 55, No. 12, 2006, pp. 1175–1178.

[17] ASTM E9-09: Standard Test Methods of Compression Testing of Metallic Materials at Room Temperature, ASTM International, West Conshohocken, PA, 2009, www.astm.org

[18] Devaraj, S., Sankaran, S., and Kumar, R., "Influence of Spark Plasma Sintering Temperature on Densification Microstructure and Mechanical Properties of a Al-4.5 wt.% Cu Alloy," *Acta Metall. Sin.*, Vol. 26, No. 6, 2013, pp. 761–771.

[19] Chaudhury, P. K. and Farghalli, A. M., "Creep and Ductility in an Al-Cu Solid Solution Alloy," *Metall. Trans. A.*, Vol. 18, No. 12, 1987, pp. 2105–2114.

[20] Kloc, L., Spigarelli, S., Cerri, E., Evangelista, E., and Longdon, T. G., "Creep Behavior of an Aluminum 2024 Produced by Powder Metallurgy," *Acta Mater.*, Vol. 45, No. 2, 1997, pp. 529–540.